Applied Surface Science 255 (2009) 3669–3675

Contents lists available at ScienceDirect

Applied Surface Science

journal homepage: www.elsevier.com/locate/apsusc

Ni/Ni_3Al interface: A density functional theory study

Cong Wang [a,*], Chong-Yu Wang [a,b]

[a] Department of Physics, Tsinghua University, Beijing 100084, PR China
[b] The International Center for Materials Physics, Chinese Academy of Sciences, Shenyang 110016, PR China

ARTICLE INFO

Article history:
Received 1 September 2008
Received in revised form 3 October 2008
Accepted 3 October 2008
Available online 17 October 2008

PACS:
05.70.Np
68.35.bd
31.15.A–

Keywords:
First-principle
Interface
Electronic structure

ABSTRACT

The optimal geometries, mechanical and thermal properties, and electronic structures of the three low index (0 0 1), (1 1 0), (1 1 1) Ni/Ni_3Al thin film were studied using first principle calculations. Simulated results indicated that Ni and Al atoms in γ' phase preferred to place in the hollow site of Ni atoms in γ phase. In hollow site models, electronic states affected by interface localize within 2 atomic layers. While the top site model, electronic states localize within 3 atomic layers. It is also found that hollow site (1 1 0) interface has the best mechanical properties. Hollow site (0 0 1) interface is the most easily formed interface, which has the best thermodynamic properties.

1. Introduction

Ni-based single crystal (SC) superalloys, which is used for turbine blades and vanes in the most advanced gas turbine engines, mainly consist of γ' precipitates coherently dispersed on a γ matrix. The γ' precipitates (an intermetallic phase of stoichiometry based upon Ni_3Al) possess an $L1_2$-type ordered face-centered cubic (fcc) structure. The γ matrix has a fcc structure. In the SC superalloys, the γ' volume fraction can reach 70% or even higher. Generally, Ni-based SC superalloys contain solutes of Cr, Co, W, Mo, Ti, Ta, etc. [1].

Solid solution precipitates, including γ' phase and γ phase, play an important role in modifying and improving properties of Ni-based SC superalloys. For interface, the host alloy and the precipitate have large influence on the properties of the materials. The morphology of the Ni_3Al strengthening phase in Ni-based SC superalloys may be altered to multilayered form via heat treatment involving eutectoid microconstituents [2–5]. Misra and Kung's method [3] permits accurately control of layer thickness at the sub-nanometer scale. In addition to unique electrical and magnetic properties, multilayered thin films display enhanced hardness and yield strength. Banerjee's work [4] pointed out that, (1 1 1) oriented multilayers are predominantly brittle and (0 0 1) oriented multilayers exhibit ductibility. Plastic deformation in such systems is confined to small volumes of material by controlling the frequency and magnitude of obstacles to dislocation motion [6,7]. Despite the richness of experimental and theoretical results, a comprehensive study on the formation energy and adhesion work of the low-index γ/γ' interfaces with DFT method is still needed. The cohesive manner, mechanical properties and thermal dynamics of γ/γ' multilayer thin film are under discussion.

In this work, density functional theory is used to simulate the γ/γ' phase interface with the indices of (0 0 1), (1 1 0), and (1 1 1). The rest of the paper is organized as follows: the model and method are described in Section 2. Results and discussion are presented in Section 3, and in Section 4, we conclude.

2. Model and methods

In this paper, the total-energy calculations were performed within the framework of the density functional theory, which is implemented in the planewave-based Vienna ab initio simulation package VASP [8,9]. In all of the calculations, the Perdew–Wang 91 exchange-correlation functional [10] within the generalized gradient approximation (GGA) is taken into account, a plane-

* Corresponding author. Tel.: +86 10 62781141; fax: +86 10 62772782.
E-mail address: wangcong00@mails.tsinghua.edu.cn (C. Wang).

0169-4332/$ – see front matter © 2008 Elsevier B.V. All rights reserved.
doi:10.1016/j.apsusc.2008.10.017

wave cutoff energy of 500.0 eV for all the models, and the electron–ion interaction potential described by the projector augmented wave method [11] are used. The k point is set to be $16 \times 16 \times 16$ for the bulk and $16 \times 16 \times 1$, $14 \times 16 \times 1$ and $8 \times 14 \times 1$ for (0 0 1), (1 1 0), and (1 1 1) interface and free surface models. The equilibrium geometry is determined by relaxation until all the forces is less than 0.04 eV/Å. The thickness of vacuum layer is 12.0 Å.

We model γ/γ' interface system with a repeated slab construction with three-dimensional translational symmetry. The sketch of our model is shown in Fig. 1. Figs. 2–4 illustrate the stacking sequence of the [0 0 1], [1 1 0], [1 1 1] orientated Ni_3Al bulk. The atomic structure of Ni bulk is the same as Ni_3Al bulk. Two series of models are considered in our calculations for (0 0 1), (1 1 0) and (1 1 1) γ/γ' interface. One is hollow site model, and the other is top site model. Interface models for Ni/Ni_3Al (0 0 1), (1 1 0) and (1 1 1) systems with Ni lattice constant matched are established where a fairly smooth coherent interface with little structural relaxation produced. The structures of interface investigated in our calculations are labeled in Fig. 5. We consider (8–56 atoms), (16–80 atoms), and (48–192 atoms) for (0 0 1), (1 1 0), and (1 1 1) interface respectively.

3. Results and analysis

We use Murnaghan equation [12]:

$$E(V) = E_0(V_0) + \frac{B_0 V_0}{B_0'(B_0' - 1)}\left[B_0'\left(1 - \frac{V_0}{V}\right) + \left(\frac{V_0}{V}\right)^{B_0'} - 1\right] \quad (1)$$

to obtain the lattice constant a_0 and the bulk modulus B_0, where the V_0 is the equilibrium volume, $E_0(V_0)$ is the cohesive energy of the ground state. V is the volume of the cell, B_0 is the bulk modulus, B_0' is the differential coefficient of the volume. The reliability of our approach is demonstrated by the excellent agreement between calculated and experimental lattice constants and bulk modulus, as listed in Table 1. γ_s is one of the basic qualities to describe stabilities of surface, which is defined as a difference between the energy of surface atoms and that of atoms in bulk [13,14] in the

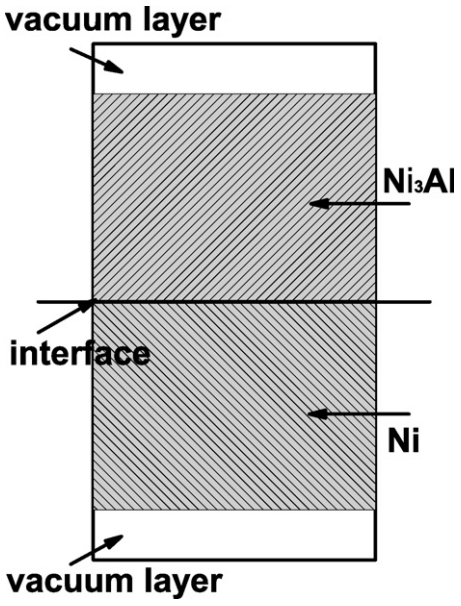

Fig. 1. The sketch of the calculated models.

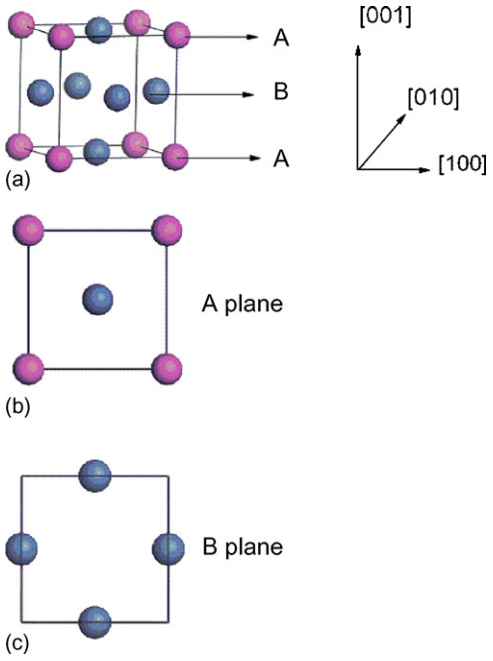

Fig. 2. Ni_3Al bulk orientated [0 0 1] direction. The purple ball denotes Al atom, and the blue ball denotes Ni atom. (a) Perfect Ni_3Al bulk with the stacking sequence (*ABABAB*. . . . .). (b) Atomic structure of *A* plane.(c) Atomic structure of *B* plane. (For interpretation of the references to colour in this figure legend, the reader is referred to the web version of the article.)

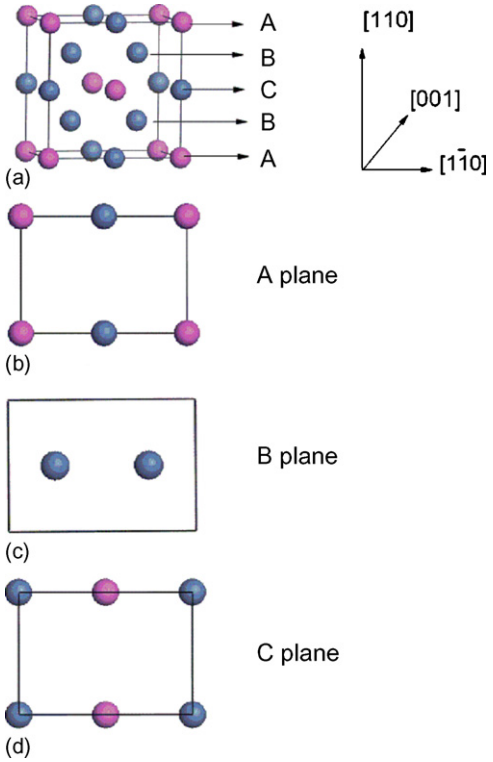

Fig. 3. Ni_3Al bulk orientated [1 1 0] direction. The purple ball denotes Al atom, and the blue ball denotes Ni atom. (a) Ni_3Al bulk orientated [1 1 0] direction, and the stacking sequence is (*ABCBABCBABCBA* . . .. .). *A* plane and *C* plane is equivalent due to the translation invariability. (b) Atomic structure of *A* plane. (c) Atomic structure of *B* plane. (d) Atomic structure of *C* plane. (For interpretation of the references to colour in this figure legend, the reader is referred to the web version of the article.)

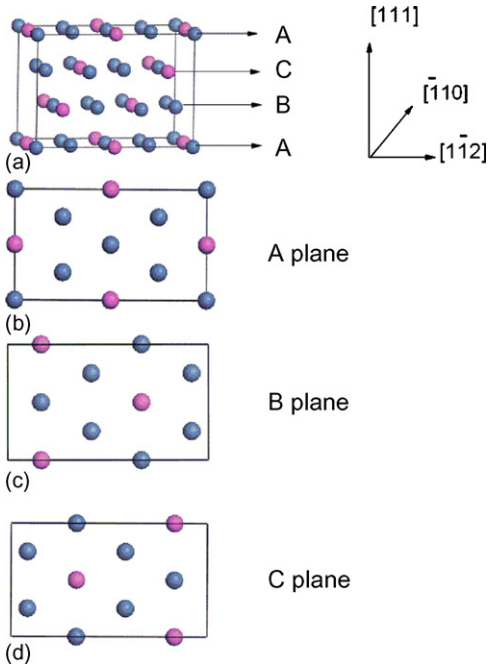

Fig. 4. Ni_3Al bulk orientated [1 1 1] direction. The purple ball denotes Al atom, and the blue ball denotes Ni atom. (a) Ni_3Al bulk orientated [1 1 1] direction, and the stacking sequence is (*ABCABCABC* . . . . .). *B* plane and *C* plane is equivalent due to the translation invariability. (b) Atomic structure of *A* plane. (c) Atomic structure of *B* plane. (d) Atomic structure of *C* plane. (For interpretation of the references to colour in this figure legend, the reader is referred to the web version of the article.)

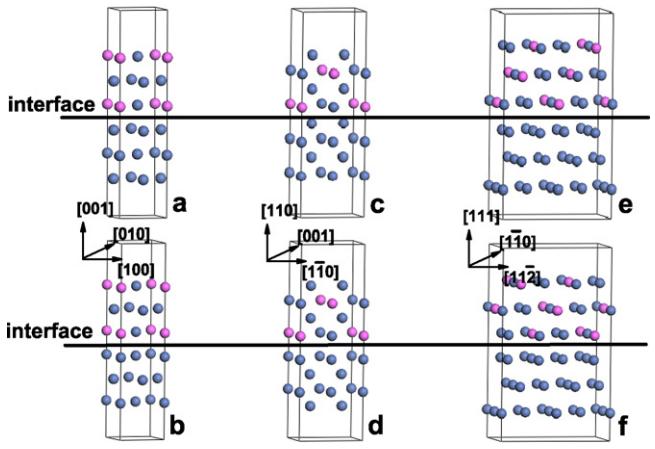

Fig. 5. The atomic structure of γ/γ' interface. Hollow site model: Ni and Al atoms in γ' phase placed in the vacancy site of Ni atoms in γ phase. Top site model: Ni and Al atoms in γ' phase placed directly on top site of Ni atoms in γ phase. The purple ball denotes Al atom, and the blue ball denotes Ni atom. (a) The hollow site (0 0 1) interface model, ([0 0 1]: γ:*ABAB* . . . . . *AB* | interface | [0 0 1]: γ':*ABAB* . . . . . *AB*) stacking. (b) The top site (0 0 1) interface model, ([0 0 1]: γ:*BABA* . . . . . *BA* | interface | [0 0 1]: γ':*ABAB* . . . . . *AB*) stacking. (c) The hollow site (1 1 0) interface model, ([1 1 0]: γ:*ABCBABCB* . . . . . *ABCB* | interface | [1 1 0]: γ':*ABCBABCB* . . . . . *ABCB*) stacking. (d) The top site (1 1 0) interface model, ([1 1 0]: γ:*BABCBABC* . . . . . *BABC* | interface | [1 1 0]: γ':*ABCBABCB* . . . . . *ABCB*) stacking. (e) The hollow site (1 1 1) interface model, ([1 1 1]: γ:*ABCABC* . . . . . *ABC* | interface | [1 1 1]: γ':*ABCABC* . . . . . *ABC*) stacking. (f) The top site (1 1 1) interface model, ([1 1 1]: γ:*ABCABC* . . . . . *ABC* | interface | [1 1 1]: γ':*CABCAB* . . . . . *CAB*) stacking. (For interpretation of the references to colour in this figure legend, the reader is referred to the web version of the article.)

Table 1
The calculated lattice constant a_0 and bulk modulus B_T. Other DFT, EAM (embedded atom method) calculated results and experiment results are listed for comparison.

	Ni		Ni_3Al	
	a_0 (Å)	B_T (GPa)	a_0 (Å)	B_T (GPa)
Our results	3.526	196.8	3.570	180.8
Other DFT results [16]	3.540	191.6	3.564	182.4
EAM results [17]	3.520	181	3.571	N/A
Experiment [18,19]	3.520	181	3.570	240.0

Table 2
The calculated γ_s (in (J/m^2)) for Ni surface. For comparison, we list other results attained by DFT, EAM and experiment.

	(1 0 0)	(1 1 0)	(1 1 1)
Our results	2.19	2.29	1.94
Other DFT results [20]	2.19	2.25	1.93
EAM results [21]	1.76	2.00	1.63
Experiments [22]		2.28 ± 0.35	

following form [15]:

$$\gamma_s \approx \frac{[E_{\text{slab}}(N) - NE_{\text{bulk}}]}{2A_s} \tag{2}$$

where $E_{\text{slab}}(N)$ is total energy of a N layer slab calculated with a sufficient large value of N, E_{bulk} denotes bulk energy, and A_s shows the corresponding surface area. Results are compared with available experimental and theoretical results as listed in Table 2, and all of the results attained from our calculations are valid.

3.1. Mechanical and thermodynamic properties

In our calculations, we use supercell model to describe interface. The supercell model introduces two free surfaces. To avoid the influence of free surface, we have to enlarge the size of model, until adhesion work of interface converges to a constant value. Adhesion work W_{ad} defined as reversible work needed to separate an interface into two slabs. Note that the critical stress required to propagate crack is given by the Griffith equation, i.e.,

$$\sigma_F = \left(\frac{W_{\text{ad}} Y}{c\pi}\right)^{1/2}$$

where σ_F is the critical stress for crack propagation, Y is the Young's modulus, c is the length of a surface crack. Thus, σ_F depends only on W_{ad}. In simulation, W_{ad} relating to mechanical properties of the considered interface can be easily determined by the following definition [23]:

$$W_{\text{ad}} = \frac{E_{\text{slab A}} + E_{\text{slab B}} - E_{A/B}}{A_i} \tag{3}$$

where $E_{A/B}$ is total energy of an A/B interface system, where there is an A/B interface between slab A and slab B, and A_i is interface area. E_{slab} is total energy of a fully relaxed slab. The results attained from our calculations are listed in Tables 3–5 . As the total length of suppercell get close to 60.0 Å, W_{ad} of all models get converged, and the corresponding total number of cells in our model "N" is 14 for (0 0 1) interface, while it is 10 and 8 for (1 1 0) and (1 1 1) interface respectively. In Tables 3–5, W_{ad} of (0 0 1), (1 1 0), and (1 1 1) hollow site model are 4.14, 4.28, and 3.69 J/m^2. While in top site models, these values are 2.31, 1.84, and 2.81 J/m^2. It is clear that $W_{\text{ad}}(0\,0\,1)_{\text{hollow}} > W_{\text{ad}}(0\,0\,1)_{\text{top}}$, $W_{\text{ad}}(1\,1\,0)_{\text{hollow}} > W_{\text{ad}}(1\,1\,0)_{\text{top}}$, and $W_{\text{ad}}(1\,1\,1)_{\text{hollow}} > W_{\text{ad}}(1\,1\,1)_{\text{top}}$. Among the three hollow site

Table 3
W_{ad} of the hollow site (0 0 1) interface model. The formation energy unit is J/m^2. N is the total number of cells used in our calculation for (0 0 1) interface.

	N						
	2	4	6	8	10	12	14
W_{ad}	4.19	4.20	4.20	4.18	4.18	4.15	4.14

Table 4
W_{ad} (J/m^2) of the hollow site (1 1 0) interface model. N is the total number of cells used in our calculation for (1 1 0) interface.

	N				
	2	4	6	8	10
W_{ad}	4.48	4.38	4.34	4.31	4.29

Table 5
W_{ad} (J/m^2) of the hollow site (1 1 1) interface model. N is the total number of cells used in our calculation for (1 1 1) interface.

	N			
	2	4	6	8
W_{ad}	3.83	3.77	3.72	3.69

Table 6
The λ_i (J/m^2) of all the interface model.

	Hollow site model	Top site model
(0 0 1)	0.12	1.95
(1 1 0)	0.15	2.60
(1 1 1)	0.16	0.94

Table 7
The interface separation of all the interface model (Å).

	Hollow site model	Top site model
(0 0 1)	1.79	2.29
(1 1 0)	1.24	2.26
(1 1 1)	2.05	2.07

models, $W_{ad}(1\,1\,0)_{hollow} > W_{ad}(0\,0\,1)_{hollow} > W_{ad}(1\,1\,1)_{hollow}$. These trends mean the hollow site model has larger cohesive strength and has larger critical stress for crack propagation than top site model. Hollow site model is more energetic stable than top site model. Among the three low index hollow site models, the adhesion work of (1 1 0) interface is larger than others, and (1 1 0) interface has the best mechanical stability. (0 0 1) interface has better mechanical property than (1 1 1) interface. On the atomic scale, the competition between brittleness and ductility takes

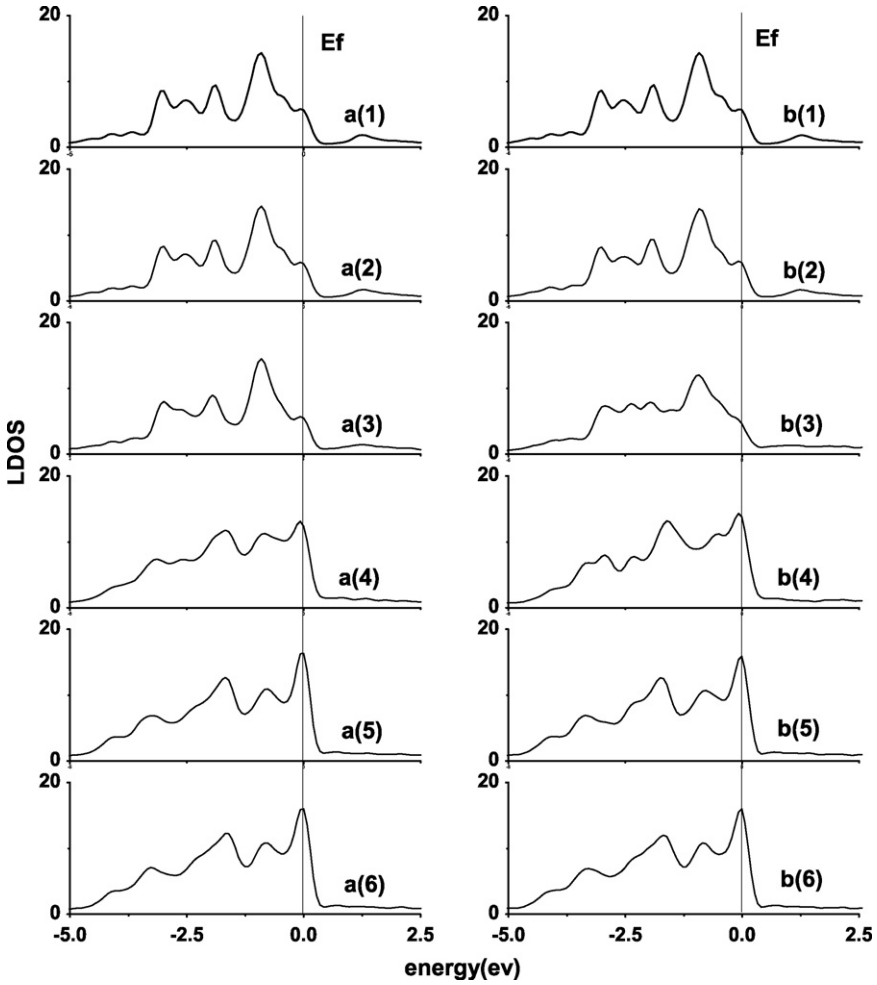

Fig. 6. LDOS of (0 0 1) interface. Fermi energy is set to be zero. a(1)–a(6) present the LDOS of hollow site interface model at γ'_{center}, $\gamma'_{sub-interface}$, $\gamma'_{interface}$, $\gamma_{interface}$, $\gamma_{sub-interface}$, γ_{center} region respectively. b(1)–b(6) present the LDOS of top site interface model at γ'_{center}, $\gamma'_{sub-interface}$, $\gamma'_{interface}$, $\gamma_{interface}$, $\gamma_{sub-interface}$, γ_{center} region respectively.

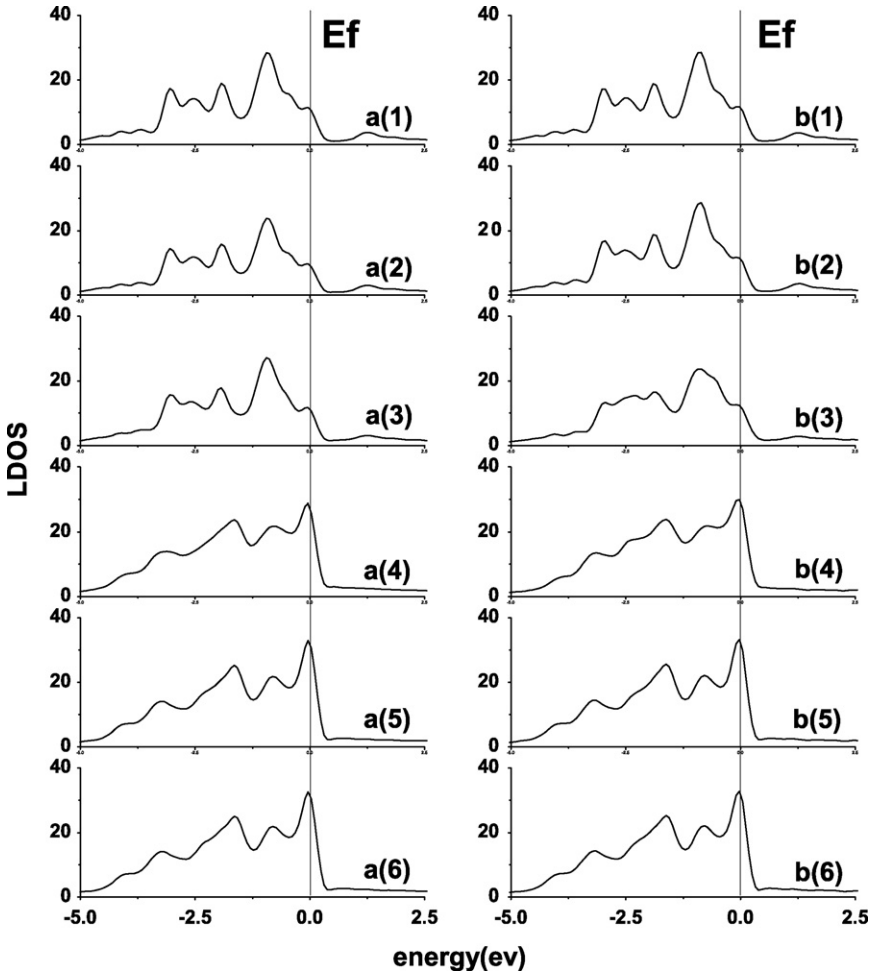

Fig. 7. LDOS of (1 1 0) interface. Fermi energy is set to be zero. a(1)–a(6) present the LDOS of hollow site interface model at γ'_{center}, $\gamma'_{sub\text{-}interface}$, $\gamma'_{interface}$, $\gamma_{interface}$, $\gamma_{sub\text{-}interface}$, γ_{center} region respectively. b(1)–b(6) present the LDOS of top site interface model at γ'_{center}, $\gamma'_{sub\text{-}interface}$, $\gamma'_{interface}$, $\gamma_{interface}$, $\gamma_{sub\text{-}interface}$, γ_{center} region respectively.

place at the crack tip, where the tensile stress is enhanced by the crack tip [24]. The competition progress of brittleness and ductility is the propagation of the crack by splitting the interface into two pieces and the emission of a dislocation. The emission of a dislocation blunts the crack and produces shielding stress which reduces the stress intensity at the crack tip. In the progress of propagating a crack, the energy required for an incremental advance in the crack front is $W(x)$. $W(x)$ is the energy release rate, x is the interface separation. When $x \to \infty$, $W(\infty) = W_{ad}$. W_{ad} of (1 1 0) interface is larger than others, and (1 1 0) interface has the best ductile properties. While the W_{ad} value of (0 0 1) interface is larger than that of (1 1 1) interface, this means (0 0 1) γ/γ' thin film has better ductile properties than (1 1 1) interface, which is agree with the experiment results [4].

Thermal stability of interface [25] is usually described by λ_i, which is commonly determined by the equation as follows [26,27]:

$$\lambda_i = \frac{[E_{A/B} - N(E_{bulkA} + E_{bulkB})]}{A_i - (\gamma_{sA} + \gamma_{sB})} \quad (4)$$

where λ_i is used to predict cohesive strength of interface systems. λ_i can be viewed as the work required to create interface from bulk materials. In contrast to the work of separation, it is not an absolute measure of interface bond strength. Instead, λ_i compares interfacial bonding strength with that of bulk material. λ_i is the excess energy of the interface, and is a crucial parameter in the process of precipitation. The precipitation kinetics is influenced by the interfacial energy between the precipitate phase and the matrix phase. Therefore, it should be an important parameter in the formation of Ni_3Al in Ni metal during sintering in which the interfaces obtain their characteristic orientations. λ_i denotes the total energy of the interfacing metal and minus the corresponding bulk energies of each [28], or a standard expression for interfacial energy.

Table 6 lists λ_i values attained from our calculations, and the relationship between different models is: $\lambda_i(0\,0\,1)_{hollow} < \lambda_i(1\,1\,0)_{hollow} < \lambda_i(1\,1\,1)_{hollow} < \lambda_i(1\,1\,1)_{top} < \lambda_i(0\,0\,1)_{top} < \lambda_i(1\,1\,0)_{top}$. This means the hollow site model has better thermodynamic stabilities than the top site model. In the process of precipitation, (0 0 1) interface is the most easily formed. From the results mentioned above, the (1 1 0) hollow site model has the largest cohesive strength, and mechanical stabilities, while the hollow site (0 0 1) interface has the best thermodynamic stabilities. This is the reason why (0 0 1) oriented γ/γ' interface is easily realized by many experiments [29].

Meanwhile, we analyse the distance of the interface separation after relaxation. The result is listed in Table 7. The distance reflects the binding properties of interface. Among varies of models, the relationship between interface separation is $d(1\,1\,0)_{hollow} < d(0\,0\,1)_{hollow} < d(1\,1\,1)_{hollow} < d(1\,1\,1)_{top} < d(1\,1\,0)_{top}$

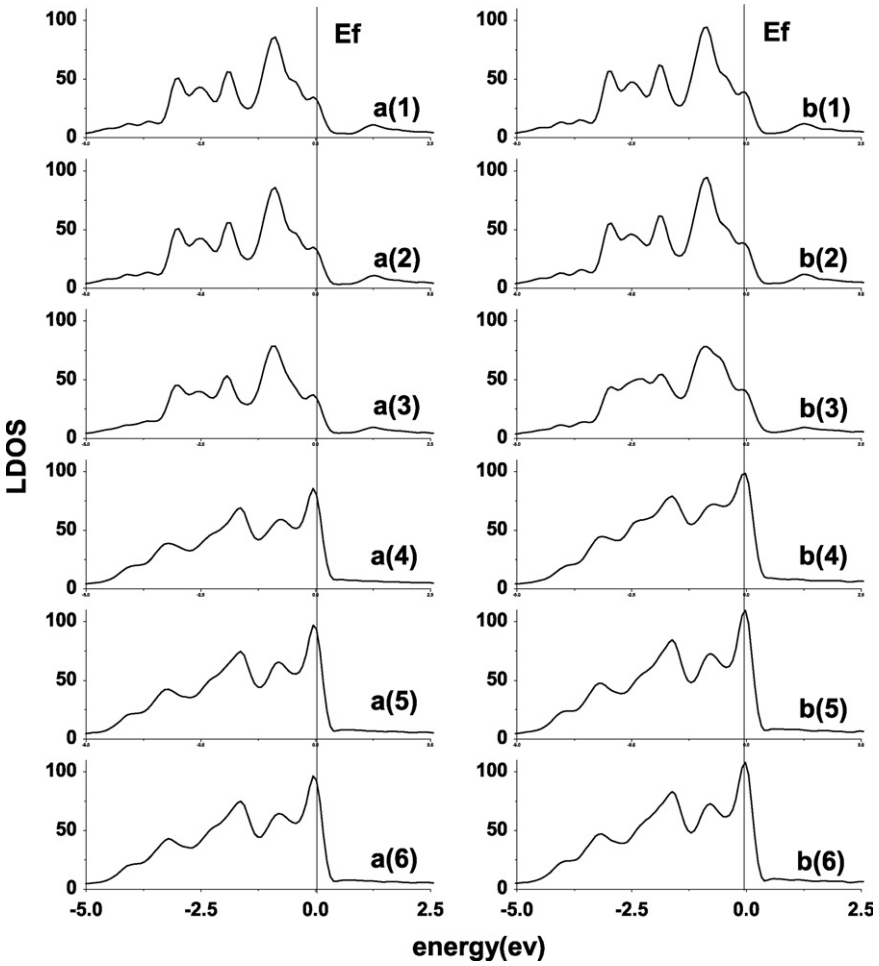

Fig. 8. LDOS of (1 1 1) interface. Fermi energy is set to be zero. a(1)–a(6) present the LDOS of hollow site interface model at γ'_{center}, $\gamma'_{sub\text{-}interface}$, $\gamma'_{interface}$, $\gamma_{interface}$, $\gamma_{sub\text{-}interface}$, γ_{center} region respectively. b(1)–b(6) present the LDOS of top site interface model at γ'_{center}, $\gamma'_{sub\text{-}interface}$, $\gamma'_{interface}$, $\gamma_{interface}$, $\gamma_{sub\text{-}interface}$, γ_{center} region respectively.

$< d(0\,0\,1)_{top}$. The recent experiment [29] provides the interface separations of (0 0 1) and (1 1 0) interfaces are 1.779 and 1.259 Å. This is in good agreement with our results.

3.2. Localized electronic state in the interface

We examined the electronic structure of the interface. Figs. 6–8 show the LDOS (localized density of state) of (0 0 1), (1 1 0) and (1 1 1) interface respectively, and as a comparison we add the LDOS of bulk Ni_3Al and Ni, which is labeled as "Ni_3Al center" or "Ni center" in the picture. For all the hollow site models, typical γ' interface electronic state has a higher peak at Fermi level (E_f), and two lowered peaks at −1.9 and −3.0 eV. As atoms get away from the interface region in γ' phase (sub-interface), these three peaks get close to the case of the bulk Ni_3Al, and finally the LDOS is the same as the bulk Ni_3Al. Typical γ phase interface electronic state has a lowered peak at Fermi level (E_f), and two lowered peaks at −1.8 and −3.1 eV. As atoms move toward the center of γ phase, the three peaks get higher. Finally, at the bulk-like Ni region, these peaks get close to the case of bulk Ni. Based on the analysis of the projected energy bands of Ni and Ni_3Al layers in hollow site models, typical γ/γ' interface electronic states are localized within 2 layers of atoms. While in the case of top site models, there exist peaks as the hollow site model, and their behavior are same. The special distribution of these electronic states lies within 3 atomic layers. This suggests that the electronic structure of top site model has larger spacial expansion, but the binding strength is weaker than hollow site model.

4. Conclusion

In this work, we use first principle calculations to investigate the three low index (0 0 1), (1 1 0) and (1 1 1) γ/γ' interfaces. And two groups of models are considered in our calculation, one is hollow site model, the other is top site model. Our results indicate that, the hollow site model has better mechanical and thermodynamic stabilities than the top site model. And among the three hollow site models, (1 1 0) interface model has larger cohesive strength and better mechanical properties. (1 1 0) interface has better ductibility. While the (0 0 1) interface model has better thermodynamic properties. The electronic states introduced by interface localized within 2 atomic layers in the hollow site model, while it is 3 atomic layers in the top site model.

Acknowledgement

This research was supported by 973 Project from the Ministry of Science and Technology of China (Grant No. 2006CB605102).

References

[1] A. Volek, F. Pyczak, R.F. Singer, H. Mughrabi, Scripta Mater. 52 (2005) 141.

[2] M.V. Nathal, R.A. MacKay, R.V. Miner, Metall. Trans. A 20A (1989) 133.
[3] A. Misra, H. Kung, Adv. Eng. Mater. 3 (4) (2001) 217.
[4] R. Banerjee, J.P. Fain, P.M. Anderson, H.L. Fraser, Scripta Mater. 44 (2001) 2629.
[5] R. Banerjee, G.B. Thompson, P.M. Anderson, H.L. Fraser, Thin Solid Films 424 (2003) 93.
[6] P.M. Anderson, T. Foecke, P.M. Hazzledine, MRS Bull. 24 (2) (1999) 27.
[7] A. Misra, J.P. Hirth, H. Kung, Philos. Mag. A 82 (16) (2002) 2935.
[8] G. Kresse, J. Hafner, Phys. Rev. B 47 (1993) R558.
[9] G. Kresse, J. Furthmller, Comput. Mater. Sci. 6 (1996) 15.
[10] J.P. Perdew, Y. Wang, Phys. Rev. B 45 (1992) 13244.
[11] P.E. Blöchl, Phys. Rev. B 50 (1994) 17953.
[12] F.D. Murnaghan, Proc. Natl. Acad. Sci. U.S.A. 30 (1944) 244–247.
[13] Q. Jiang, H.X. Shi, M. Zhao, Acta Mater. 47 (1999) 2109.
[14] Q. Jiang, H.X. Shi, M. Zhao, Acta Mater. 49 (2001) 3143.
[15] V. Fiorentini, M. Methfessel, J. Phys.: Condens. Matter 8 (1996) 6525.
[16] Y. Wang, Z.-K. Liu, L.-Q. Chen, Acta Mater. 52 (2004) 2665.
[17] Y. Mishin, Acta Mater. 52 (2004) 1451.
[18] Available from: ¡ http://www.webelements.com/¿.
[19] A.B. Kamara, A.J. Ardell, C.N.J. Wagner, Metall. Mater. Trans. A 27 (1996) 2888.
[20] F. Mittendorfer, A. Eichler, J. Hafner, Surf. Sci. 423 (1999) 1–11.
[21] A. Volek, F. Pyczak, R.F. Singer, H. Mughrabi, Scripta Mater. 572 (2005) 141.
[22] L.E. Murr, Interfacial Phenomena in Metals and Alloys, Addison-Wesley, Reading, MA, 1975.
[23] M.W. Finnis, J. Phys.: Condens. Matter 8 (1996) 5811.
[24] C.E. Inglis, Trans. Inst. Naval Arch. 55 (1913) 219.
[25] D. Myers, Surfaces, Interfaces, and Colloids: Principles and Applications, 2nd ed., John Wiley & Sons, Inc., New York, 1999, pp. 8C14.
[26] J.H. van der Merwe, Prog. Surf. Sci. 67 (2001) 365.
[27] M. Christensen, S. Dudiy, G. Wahnström, Phys. Rev. B 65 (2002) 045408.
[28] J.R. Smith, W. Zhang, Acta Mater. 48 (2000) 4395.
[29] M. Lachowicz, W. Dudziński, M. Podrez-Radziszewska, Mater. Charact. 59 (2008) 560.